

arXiv:1802.03489v2 [physics.ins-det] 12 Aug 2018

arXiv:1802.03489 v2[物理学报]2018 年 8 月 12 日

Signal-background discrimination with convolutional neural networks in the PandaX-III experiment using MC simulation

基于蒙特卡罗模拟的 panDax-iii 实验中卷积神经网络信号背景识别

Hao Qiao, Chunyu Lu, Xun Chen^{*}, Ke Han, Xiangdong Ji, and and Siguang Wang [†]

乔浩、于春、鲁迅、Chen^{*}、汉克、冀向东和王四光

School of Physics and State Key Laboratory of Nuclear Physics and Technology and Center for High Energy Physics, Peking University, Beijing 100871, China INPAC and School of Physics and Astronomy, Shanghai Jiao Tong University, Shanghai Laboratory for Particle Physics and Cosmology, Shanghai 200240, China T.D. Lee Institute, Shanghai 200240, China

北京大学物理学院和核物理与技术国家重点实验室及高能物理中心, 北京 100871, 中国 INPAC, 上海交通大学物理与天文学院, 上海粒子物理与宇宙学实验室, 上海 200240, 中国李东堂研究所, 上海 200240

August 14, 2018

2018 年 8 月 14 日

Abstract

摘要

The PandaX-III experiment will search for neutrinoless double beta decay of Xe with high pressure gaseous time projection chambers at the China Jin-Ping underground Laboratory. The tracking feature of gaseous detectors helps suppress the background level, resulting in the improvement of the detection sensitivity. We study a method based on the convolutional neural networks to discriminate double beta decay signals against the background from high energy gammas generated by Bi and Tl decays based on detailed Monte Carlo simulation. Using the 2-dimensional projections of recorded tracks on two planes, the method successfully suppresses the background level by a factor larger than 100 with a high signal efficiency. An improvement of 62% on the efficiency ratio of $\nu\nu s/ p\Rightarrow b$ is achieved in comparison with the baseline in the PandaX-III conceptual design report.

潘达克斯三号实验将在中国金平地下实验室用高压气体时间投影室寻找氙的无中微子双 β 衰变。气体探测器的跟踪特性有助于抑制背景水平, 从而提高探测灵敏度。基于详细的蒙特卡罗模拟, 我们研究了一种基于卷积神经网络的方法来区分背景双 β 衰变信号和铋、铊衰变产生的高能 γ 。该方法利用记录轨道在两个平面上的二维投影, 以高信号效率成功地将背景电平抑制大于 100 倍。与 PandaX-III 概念设计报告中的基线相比, $\nu\nu s/ p\Rightarrow b$ 的效率比提高了 62%。

neutrino, double beta decay, convolutional neural networks, background suppression PACS number(s): 14.60.Pq, 23.40.-s, 07.05.Mh

中微子, 双 β 衰变, 卷积神经网络, 背景抑制 PACS 数: 14.60.Pq, 23.40.-s, 07.05.Mh

1 Introduction

1 引言

The Dirac or Majorana nature of neutrinos is one of the most fundamental questions in particle physics. The conservation of the lepton number will be violated if neutrinos are Majorana fermions, which is intricately related to the matter-antimatter asymmetry in our universe [1]. The so-called neutrinoless double beta decay (NLDBD) process, in which a nucleus with even atomic number Z and even neutron number N emits two electrons simultaneously without neutrinos, is possible if neutrinos are Majorana. Therefore experimental identification of such rare process would be an important breakthrough of particle physics. Xe is a widely used isotope in experiments searching for NLDBD due to its high abundance in natural xenon and relatively low cost of enrichment. Experiments using this target include KamLAND-Zen [2], EXO-200 [3], and NEXT [4].

中微子的狄拉克或马约纳性质是粒子物理学中最基本的问题之一。如果中微子是马约纳费米子，轻子数的守恒将被破坏，这与我们宇宙中物质反物质的不对称性密切相关，[1]。所谓的无中微子双 β 衰变(NLDBD)过程，其中一个具有偶数原子序数 Z 和偶数中子序数 N 的原子核在没有中微子的情况下同时发射两个电子，如果中微子是马约那(Majorana)，这是可能的。因此，对这种罕见过程的实验鉴定将是粒子物理学的一个重要突破。Xe是一种广泛应用于寻找NLDBD实验的同位素，因为它富含天然氙，富集成本相对较低。使用该目标的实验包括卡姆兰-禅宗[2号、EXO-200 [3号和下一个[4号]。

The PandaX-III project plans to construct a ton-scale NLDBD experiment in the China Jin-Ping underground Laboratory (CJPL) using time projection chambers (TPCs) filled with high pressure xenon gas with enriched Xe [5]. The first detector will have 200 kg xenon gas at 10 bar pressure and read out ionized electrons directly with Micromegas (Micro-MESH Gaseous Structure) detectors. Trimethylamine (TMA) mixed with xenon converts part of the scintillation in xenon to ionization and improves energy resolution of the TPC. The energy resolution at Xe NLDBD Q-value (2.458 MeV) is expected to reach 3% (Full-Width-Half-Maximum, FWHM). The admixture also suppresses deconvolution of ionized electrons and improves the tracking capability.

潘达克斯三号项目计划在中国金平地下实验室(CJPL)建造一个吨级的非视距实验，使用装有高压氙气和富氙[5号的时间投影室。第一个探测器将有200公斤10巴压力的氙气，并直接用微型气体结构探测器读出电离电子。三甲胺与氙混合后将氙中的部分闪烁转化为电离，提高了热释光探测器的能量分辨率。Xe NLDBD Q值(2.458兆电子伏)下的能量分辨率预计将达到3%(全宽半高，FWHM)。混合物还抑制电离电子的deconvolution并提高跟踪能力。

The main backgrounds in the Region of Interest (ROI) of PandaX-III are high energy gamma rays from the decay of Bi (2.447 MeV) and Tl (2.614 MeV) in the detector materials. These background events may fall in the same energy window of NLDBD Q-Value and mimic a signal event. The high pressure gaseous TPC is capable of recording the tracks of ionizing particles within

潘达克斯-iii 感兴趣区域的主要背景是探测器材料中铋(2.447兆电子伏)和铊(2.614兆电子伏)衰变产生的高能伽马射线。这些背景事件可能落在NLDBD Q值的同一能量窗口中，并模拟信号事件。高压气态热塑性塑料能够记录内部电离粒子的轨迹

✉Corresponding author: chenxun@sjtu.edu.cn †Corresponding author: siguang@pku.edu.cn

✉Corresponding 作者: chenxun@sjtu.edu.cn 对应作者: siguang@pku.edu.cn

it, providing additional information about the events besides the total energy depositions. Electrons with energy of 1 MeV travel in average 10 cm in the PandaX-III detector. At the end of an electron trajectory, the energy loss per unit length (dE/dx) increases dramatically, known as Bragg peak. NLDBD will have two simultaneous electron tracks in different directions and thus two distinctive Bragg peaks. This feature can be used to distinguish the NLDBD signal from gamma backgrounds. The topological signatures of Xe NLDBD events and gamma rays have been studied by the NEXT collaboration [6, 7], and an extra background rejection factor is achieved by reconstructing the tracks and identifying the end point energies. It is expected that similar method could provide a background rejection factor of 35, which serves as a baseline in PandaX-III.

它提供了除总能量沉积之外的关于事件的附加信息。能量为 1 兆电子伏的电子在潘达克斯-iii 探测器中平均行进 10 厘米。在电子轨迹的末端，单位长度的能量损失(dE/dx)急剧增加，称为布拉格峰。NLDBD 将在不同方向同时有两条电子轨道，因此有两个不同的布拉格峰。该特征可用于区分自然背景和伽马背景。Xe NLDBD 事件和伽马射线的拓扑特征已经由下一次合作[6, 7]进行了研究，并且通过重建轨迹和识别终点能量获得了额外的背景抑制因子。预计类似的方法可以提供 35 的背景抑制因子，这是第三代聚苯胺的基线。

The topological particle identification method, like other traditional event classification methods used in particle physics, requires the reconstruction of designed expert features of the events with sophisticated algorithms for signal classification. The usage of deep neural networks in the particle physics for classification without the aid of designed features has been explored in recent years, and outstanding performance has been obtained[8, 9]. Convolutional neural networks (CNN), an artificial neural network originally developed for image analysis, have gained popularity in particle physics experiments these years [10, 11, 12, 13, 14]. CNN is especially suited for signal-background discrimination of electron tracks in the gaseous TPC. The NEXT collaboration has studied the background rejection power of CNN in the search of NLDBD by using images with all three dimensional projections of the tracks, and obtained an improvement compared with the method based on the same topological information [15]. But such a method cannot be used in the first phase of PandaX-III directly due to its strip readout. An alternative way of data preparation should be considered.

拓扑粒子识别方法与粒子物理中使用的其他传统事件分类方法一样，需要用复杂的信号分类算法重建事件的设计专家特征。近年来，人们探索了在没有设计特征的情况下将深度神经网络用于粒子物理的分类，并获得了[8, 9]的优异性能。卷积神经网络(美国有线电视新闻网)，一种最初为图像分析开发的人工神经网络，近年来在粒子物理实验中获得了广泛的应用，[10, 11, 12, 13, 14]。有线电视新闻网特别适用于气态热塑性塑料中电子轨迹的信号背景鉴别。下一步的合作研究了有线电视新闻网在利用所有三维轨迹投影的图像搜索自然语言数据库时的背景抑制能力，并与基于相同拓扑信息的方法[5 相比得到了改进。但是这种方法不能直接用于第一阶段的潘达克斯-三，因为它的条形读出。应考虑另一种数据准备方式。

In this work, we apply the CNN technique to the signal and background discrimination in the PandaX-III experiment, based on a detailed Monte Carlo (MC) simulation with detector geometry and realistic drifting of ionized electrons. This article is organized as follows. In Sec.2, we give a brief introduction to the PandaX-III detector and the properties of NLDBD events in it. In Sec.3, we describe the simulation of NLDBD events in PandaX-III. Then we introduce the method of classification of NLDBD signals and backgrounds with convolutional neural networks in Sec.4. We present the results based on Monte Carlo simulation in Sec.4.3. A short summary is given in the last section.

在这项工作中，我们将美国有线电视新闻网技术应用于潘达克斯-三号实验中的信号和背景识别，基于一个详细的蒙特卡罗模拟与探测器几何形状和电离电子的真实漂移。本文组织如下。秒。2、简要介绍了PanDax-iii 探测器及其内 NLDBD 事件的性质。秒。3、我们描述了潘达克斯三号中的 NLDBD 事件的模

拟。然后介绍了利用卷积神经网络对非线性数字信号和背景进行分类的方法。4.我们以秒为单位给出了基于蒙特卡罗模拟的结果。4.3 .最后一节给出了一个简短的总结。

2 The PandaX-III detector and background suppression

2 PanDax-iii 探测器和背景抑制

A detailed introduction to the PandaX-III detector can be found in the conceptual design report (CDR) [5]. A high pressure gaseous TPC is adopted due to its higher energy resolution in comparison with liquid detectors, and the capability of imaging the electron tracks. Deposited energy inside the TPC will be released in the form of scintillation light and ionized electrons. The electrons will drift towards the ends of the TPC due to the strong electric field and be finally collected by the readout planes. The first TPC module will be filled with 200 kg 90% enriched Xe with 1% TMA mixture. In the second phase, the ton-scale experiment will have 5 independent detector modules, each of which will contain 200 kg of xenon gas.

潘达克斯-iii 探测器的详细介绍可在[5]概念设计报告中找到。采用高压气态热塑性塑料是因为它比液体探测器具有更高的能量分辨率和对电子轨迹成像的能力。热塑性塑料内部沉积的能量将以闪烁光和电离电子的形式释放。由于强电场，电子将向热塑性塑料的末端漂移，并最终被读出平面收集。第一个热塑性塑料组件将填充 200 千克 90% 浓缩 Xe 和 1% TMA 混合物。在第二阶段，吨级实验将有 5 个独立的探测器模块，每个模块将包含 200 公斤氙气。

The mixed gas of 10 bar pressure will be enclosed in an Oxygen-Free High Conductivity (OFHC) copper pressure vessel of cylindrical shape with a length about 2 m and diameter about 1.5 m. The total volume of the vessel is about 3.5 m. A cylindrical TPC, with two drift regions separated by a cathode plane in the middle, will be placed inside the vessel. Each drift region will have a drift length of about 1 m and a design drift field of 1000 V/cm, shaped by the field cage. Two options to build the cylindrical field cage have been considered. The classical design with copper rings has been used widely in other experiments, including the PandaX-I [16] and PandaX-II [17] dark matter experiments. This option will be the baseline design of PandaX-III and it has been used in all our MC simulations. Another design using Diamond-Like-Carbon (DLC) coated on Kapton films may reduce difficulties during the construction and overall background rate. This approach is currently under active R&D within PandaX-III collaboration.

10 巴压力的混合气体将被封装在长度约为 2 米、直径约为 1.5 米的圆柱形无氧高电导率(OFHC)铜压力容器中。容器的总体积约为 3.5 米。将在容器内放置圆柱形热塑性塑料，其中两个漂移区由中间的阴极平面隔开。每个漂移区的漂移长度约为 1 米，设计漂移场为 1000 伏/厘米，由场笼决定。已经考虑了建造圆柱形磁场笼的两种选择。铜环的经典设计已被广泛用于其他实验，包括潘达克斯-i[16]和潘达克斯-ii[17]暗物质实验。这个选项将是潘达克斯-3 的基线设计，它已经用于我们所有的大规模计算机模拟。另一种使用涂覆在 Kapton 薄膜上的类金刚石碳(DLC)的设计可以减少建造过程中的二次污染和整体背景率。这种方法目前正在泛达三号合作框架内由 R&D 积极实施。

A special realization of Micromegas, called Microbulk, will be used in the first phase of PandaX-III to detect the ionization electrons. An excellent energy resolution of 3% Full-Width-Half-Maximum (FWHM) at the NLDBD Q-value is expected based on R&D results at 10 bar of Xe with TMA by the T-REX project [18]. Each readout plane of the PandaX-III detector will be covered by 41 specially designed 20 → 20 cm Microbulk Micromegas (MM) modules, and each module will be read out by 128 channels of X-Y strips of 3 mm pitch (64 in each direction). The total number of readout channels is about 10000.

微型探测器(Micromegas)的一种特殊实现，称为微型探测器(Microbulk)，将在 PandaX-III 的第一阶段用于探测电离电子。根据[霸王龙项目 18]在 10 巴 Xe 和 TMA 下的 R&D 结果，预计在 NLDBD Q 值下

具有 3%全宽-半最大值(FWHM)的出色能量分辨率。PandaX-III 探测器的每个读出平面将被 41 个专门设计的 20 → 20 厘米微体积(MM)模块覆盖, 每个模块将被 128 个 3 mm 间距的 X-Y 条通道读出(每个方向 64 个)。读出通道的总数约为 10000 个。

According to the detailed Geant4 [19, 20] based MC simulation, the main background contributions come from the high energy gamma rays generated by the radioactive descendants of U and

根据基于 Geant4 [19, 20]的详细蒙特卡罗模拟, 主要的背景贡献来自于铀和铀的放射性后代产生的高能伽马射线

See Appendix A

见附录一

2

2

Th inside the detector [5].Steel bolts and MM modules contribute to the majority of the backgrounds within the energy window of $(Q - 2, Q + 2)$, where is the corresponding standard deviation at the expected detector resolution of 3%.By assuming the input material activity and taking the electron diffusion and the detector response into consideration, the background index (BI) is about $3 \rightarrow 10$ counts/(keV kg year) [5].That means that about 70 background events would be observed in the energy windows each year, which is too high for a NLDBD experiment.

这在探测器[5]内部。钢螺栓和金属模块构成了能量窗 $(Q - 2, Q + 2)$ 内的大部分背景, 在预期探测器分辨率为 3%时, 相应的标准偏差为多少。通过假设输入材料的活性并考虑电子扩散和探测器响应, 背景指数(BI)约为 $3 \rightarrow 10$ 计数/(keV kg 年)[5]。这意味着每年在能量窗口中会观察到大约 70 个背景事件, 对于 NLDBD 实验来说, 这是太高了。

Topological information of an event track, such as track length, shape, and energy deposition per unit distance, can help suppress background events further.This powerful background suppression capability has been demonstrated by other studies [18, 7].The two high energy electrons produced in the NLDBD process will generate large amount of ionization electrons along their path inside the high pressure xenon gas and lose energy quickly, generally resulting in tracks with length of about 15 cm and higher energy depositions at the ends due to the Bragg peaks of electrons.The gamma background loses energy mostly through Compton scattering or photoelectric interactions, and the number of tracks may vary.Ideally, such topological information can be easily used if the track is fully reconstructed in 3D spaces.In the first phase of PandaX-III, the z position of the energy deposition, characterizing the drifting time of electrons, can be extracted easily.But the xy position on the readout plane can not be determined exactly because of the ambiguity introduced by multiple strip signals at the same time.Though the 3D reconstruction is difficult, the projection of the tracks in the xz and yz will be easily acquired.It is necessary to find out a method to make use of all the information from this incomplete tracking in order to better discriminate signal and background.

事件轨迹的拓扑信息, 如轨迹长度、形状和单位距离的能量沉积, 有助于进一步抑制背景事件。这种强大的背景抑制能力已被[18, 7]的其他研究证明。NLDBD 过程中产生的两个高能电子将在高压氙气中沿其路径产生大量电离电子, 并迅速失去能量, 由于电子的布拉格峰, 通常导致长度约为 15 cm 的轨道和在末端更高能量的沉积。伽马背景主要通过康普顿散射或光电相互作用损失能量, 轨道数量可能会变化。理想情况下, 如果在 3D 空间中完全重建轨迹, 则可以很容易地使用这种拓扑信息。在 PanDax-iii 的第一阶段, 表征电子漂移时间的能量沉积的 z 位置可以很容易地提取出来。但是读出平面上的 xy 位置不能

被精确地确定，因为多个条形信号同时引入了模糊性。虽然 3D 重建是困难的，但是在 xz 和 yz 中轨道的投影将容易获得。为了更好地区分信号和背景，有必要找到一种方法来利用这种不完全跟踪的所有信息。

3 Simulation of NLDBD events in PandaX-III

3 潘达克斯-三号卫星中的 NLDBD 事件模拟

The study was carried out with MC simulation events. BambooMC, a MC program based on the Geant4 toolkit, was used to perform detailed simulation of tracking of electrons and gamma within the PandaX-III detector. The detailed structure of the detector module, including the copper vessel, the gas mixture, the field cage with copper rings and the readout planes, was constructed in the simulation (see Fig. 1). The gas mixture contains 99% (mass fraction) Xe enriched (at the level of 90%) xenon gas and 1% TMA. The electric field of 1000 V/cm along the z direction was also applied in the simulation.

这项研究是通过模拟事件进行的。竹子监测中心是一个基于 Geant4 工具包的监测中心项目，用于对 PanDax-iii 探测器内的电子和伽马射线进行详细的跟踪模拟。探测器模块的详细结构，包括铜容器、气体混合物、带有铜环的场笼和读出平面，在模拟中构建(见图 1)。气体混合物含有 99%(质量分数)的富氙(含量为 90%)氙气和 1%三氧化二甲烷。模拟中还应用了沿 z 方向的 1000 伏/厘米的电场。

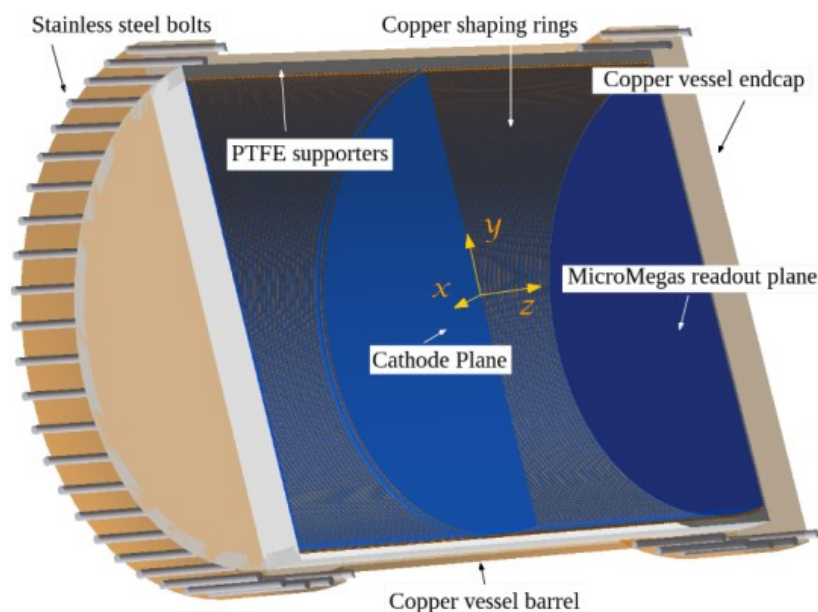


Figure 1: A cross-sectional view of the simulated PandaX-III detector.

图 1: 模拟 PanDax-iii 探测器的横截面图。

The DECAY0 package [21] was used to generate the NLDBD signal events, each contains two electrons with a total kinetic energy around the Q -value. These events were sampled uniformly inside the gas mixture within the TPC. For the backgrounds, gamma with the energy of 2447.7 keV (from Bi) and 2614 keV (from Tl) are sampled from the copper vessel volume with an isotropic angular distribution.

DECAY0 组件[21]用于产生 NLDBD 信号事件，每个事件包含两个电子，总动能约为 Q 值。这些事件在热塑性塑料内的气体混合物中均匀取样。对于背景，能量为 2447.7 千电子伏(来自铋)和 2614 千电子伏(来自铊)的伽马以各向同性角度分布从铜容器体积中取样。

After the simulation, the information of particle energy depositions inside the TPC, including the position, time, energy and particle type, were recorded in the output file, serving as the input of the following digitization step. Each readout channel's waveform, expressed by a time series of electrons arriving the corresponding area in the readout plane, was generated by simulating the generation, drifting and diffusion of the ionization electrons during the digitization.

模拟后，TPC 内部的粒子能量沉积信息，包括位置、时间、能量和粒子类型，被记录在输出文件中，作为后续数字化步骤的输入。每个读出通道的波形由到达读出平面中相应区域的电子的时间序列表示，通过模拟数字化过程中电离电子的产生、漂移和 diffusion 产生。

3

3

For each energy deposition, the number of ionization electrons is randomly sampled with the W-value of 21.9 eV and Fano factor of 0.14 [22]. The drifting velocity and diffusion parameters of ionization electrons were calculated with the Magboltz [23] package through the interface of Garfield++ [24] by taking the constituent of the gas mixture and electric field into consideration. In this study, we continued to use the drifting velocity of 1.87 mm/s, the transverse diffusion parameter of $1.02 \rightarrow 10 \text{ cm}$ and the longitudinal diffusion parameter of $1.39 \rightarrow 10 \text{ cm}$ [5].

对于每一次能量沉积，电离电子的数量是随机取样的，其钨值为 21.9 电子伏，费诺系数为 0.14 [22]。考虑到气体混合物的成分和电场，通过 Garfield++ [24] 的界面，用 Magboltz [23] 包计算离子电子的漂移速度和 diffusion 参数。在这项研究中，我们继续使用 1.87 毫米/秒的漂移速度， $1.02 \rightarrow 10 \text{ cm}$ 的横向 diffusion 参数， $\rightarrow 10 \text{ 厘米}$ [5] 的纵向 diffusion 参数。

For each ionization electron, the time and position when it arrives the readout plane is calculated with the initial position of the energy deposition together with the parameters. Then the possible fired readout channel is determined according to the arrangement of the MM modules and channels. The electron loss during the drifting is ignored. In real experiment, the gas will be purified continuously by the online recycling system.

对于每个电离电子，它到达读出平面的时间和位置是用能量沉积的初始位置和参数计算的。然后，根据毫米模块和通道的排列确定可能激发的读出通道。漂移过程中的电子损失被忽略。在实际实验中，气体将通过在线回收系统连续净化。

We obtained a set of time series of recorded electron number for all the readout channels after iterating all the depositions in the TPC. The width of the time bin is determined assuming a sampling rate of 5 Ms/sec. An example of such a time series is shown in Fig. 2. Because the readout window is limited to 102.4 s (512 time bins) and the maximum drifting time in one chamber of the PandaX-III TPC is about 535 s, the waveforms may contain only part of the long time series. To simulate the trigger, We used the integrated energy, which is translated from the number of electrons, in a sliding window of 256 bins along the time axis, as a trigger. The event is "triggered" when the energy exceeds $Q/2 = 1.229 \text{ MeV}$. Two hundred fifty-six bins before the trigger signal and 256 bins after are kept in the final waveform. These waveforms simulate the outputs from real detector electronics. The summation of the total number of electrons are translated directly into the readout energy without additional smearing applied.

我们在重复全光子晶体中的所有沉积之后，获得了所有读出通道的一组记录电子数的时间序列。假设采样速率为 5 毫秒/秒，则确定时间仓的宽度。这种时间序列的例子如图 2 所示。因为读出窗口被限制为 102.4 秒(512 个时间仓)，并且在 PandaX-III TPC 的一个腔室中的最大漂移时间大约为 535 秒，所以波形可以仅包含长时间序列的一部分。为了模拟触发器，我们使用积分能量作为触发器，该积分能量是从

沿着时间轴的 256 个仓的滑动窗口中的电子数量转换而来的。当能量超过 $Q/2=1.229$ 兆电子伏时，该事件被“触发”。触发信号之前的 256 个仓和之后的 256 个仓被报告在最终波形中。这些波形模拟真实探测器电子器件的输出。电子总数的总和被直接转换成读出能量，而无需施加额外的拖尾。

After the detailed simulation and digitization, we found the detection efficiency of NLDBD signal is 56.2% within the energy window of $Q/2$, i.e., [2395, 2520] keV, assuming a detector resolution of 3% full width half maximum (FWHM). The value is consistent with that reported in the PandaX-III CDR.

经过详细的模拟和数字化后，我们发现，假设探测器分辨率为 3% 全宽半高(FWHM)，在 $Q/2$ 的能量窗口内，即 [2395, 2520] keV 内，NLDBD 信号的探测效率为 56.2%。该值与第三代化学药品报告中报告的值一致。

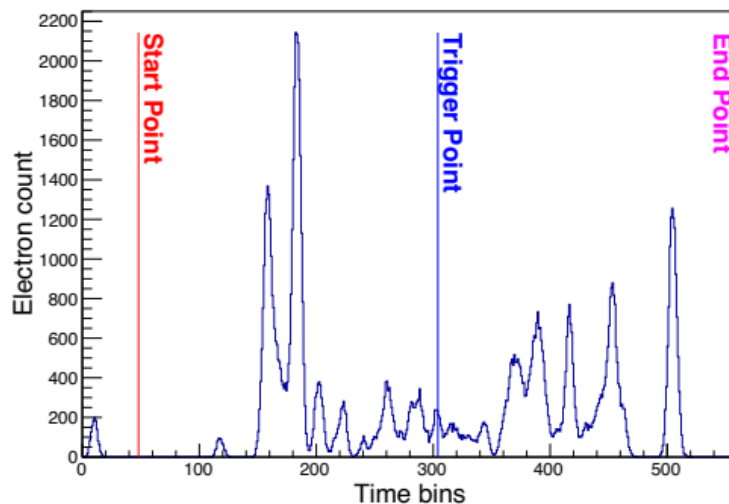


Figure 2: The number of electrons hitting a readout plane in an event by time. The bin width is 20ns. Time 0 is defined as the time when the first electron reaches the readout plane. The time series between the start point and the end point are finally recorded.

图 2: 在一个事件中，电子按时间撞击读出平面的数量。箱子宽度是 20ns。时间 0 定义为第一个电子到达读出平面的时间。最终记录起点和终点之间的时间序列。

4 Event Classification with CNN

4 有线电视新闻网事件分类

The rapid development and application of the deep neural networks, especially the usage of CNN in image classification in recent years [25, 26], provide a possibility for the discrimination of signal and background in PandaX-III without fully reconstructing the tracks.

深度神经网络的快速发展和应用，特别是近年来有线电视新闻网在图像分类中的应用，[25, 26]，为在不完全重构轨迹的情况下识别 PanDax-iii 中的信号和背景提供了可能。

4.1 Introduction of CNN

4.1 有线电视新闻网简介

A detailed introduction to the CNN can be found in Ref.[26].We introduce the basic ideas here.Similar to the ordinary neural networks, the basic block of CNNs is neuron, which generates output value according to the input and its own parameters.Neurons are grouped into layers by their different functionalities, and the network is a stacking of the layers.Each layer of the network can be regarded as a non linear tranformation that maps a tensor(multidimensional arrays) to another

美国有线电视新闻网的详细介绍见参考文献。[26]。我们在这里介绍基本概念。与普通神经网络相似，神经网络的基本块是神经元，神经元根据输入和自身参数产生输出值。神经元通过它们的 different 功能被分成层，网络是层的堆叠。网络的每一层都可以看作是一个非线性变换，将张量(多维数组)映射到另一个

4

4

tensor, so the whole network is mostly like a complicated transformation which tries to fit the input tensors to the output tensors.

张量，所以整个网络就像一个复杂的变换，试图将输入张量与输出张量相匹配。

CNNs are specially designed to work with image data, by reducing the parameter space with "convolution".The first layer of a CNN reads data from images of certain size, and the last layer generates the result of classification by arranging all neurons in a row.A CNN may contain one or more convolutional layers, in which each neuron is used to compute the dot product (convolution) of its weight and values from a small region in the input volume.With such structures, CNNs are capable of learning features from given images during the training procedure so that they can be used to classify new images by recognizing their features with the same algorithm.

有线电视新闻网是专门为处理图像数据而设计的，通过“卷积”减少了参数空间。有线电视新闻网的第一层从一定大小的图像中读取数据，最后一层通过将所有神经元排成一行来产生分类结果。有线电视新闻网可以包含一个或多个卷积层，其中每个神经元用于从输入体积的小区域计算其权重和值的点积(卷积)。利用这种结构，中枢神经系统能够在训练过程中从给定的图像中学习特征，从而能够通过用相同的算法识别新图像的特征来对新图像进行分类。

It was shown that significant improvement on the performance had been achieved with higher network depth [27].But a degradation problem appears when the network becomes deeper, together with higher training error [28].The residual network (ResNet), introduces shortcut connections between nonadjacent layers to mitigate the problem [29] and shows outstanding performance.In our study, we used the 50-layer ResNet-50 within the Keras [30] deep learning library.The input and output layers of the network have been modified so that it can accept our input data and generate an output value between 0 (exact background) and 1 (exact signal).The detailed network structure is given in Table 1.

结果表明，随着网络深度的增加，[27]的性能得到了显著提高。但是当网络变得更深时，就会出现退化问题，以及更高的训练误差[28]。剩余网络(ResNet)引入了不相邻层之间的快捷连接，以缓解[29]的问题，并显示出出色的性能。在我们的研究中，我们使用了喀拉拉[30]深度学习图书馆的 50 层 ResNet-50。网络的输入和输出层已经过修改，因此它可以接受我们的输入数据，并生成介于 0(精确背景)和 1(精确信号)之间的输出值。表 1 给出了详细的网络结构。

layer name layer type output tensor layer attribute repetition input 1 InputLayer 240, 240, 3 conv1 block Convolution2D 120, 120, 64 7→7, 64 pooling MaxPooling2D 59, 59, 64 conv2 block

图层名称 图层类型 输出张量 图层属性 重复输入 1 输入 图层 240、240、3 conv1 块 卷积 2D
120、120、64 7→7、64 池 maxpooling2d 59、59、64 conv2 块

Convolution2D 59, 59, 64 1→1, 64

卷积 2D 59, 59, 64 1→1, 64

→3, 64 3 Convolution2D 59, 59, 64 3

→3, 64 3 convolution2d 59, 59, 64 3

Convolution2D 59, 59, 256 1→1, 256

卷积 2D 59, 59, 256 1→1, 256

conv3 block

conv3 块

Convolution2D 30, 30, 128 1→1, 128

卷积 2D 30, 30, 128 1→1, 128

→3, 128 4 Convolution2D 30, 30, 128 3

→3, 128 4 convolution2d 30, 30, 128 3

Convolution2D 30, 30, 512 1→1, 512

卷积 2D 30, 30, 512 1→1, 512

conv4 block

conv4 块

Convolution2D 15, 15, 256 1→1, 256

卷积 2D 15, 15, 256 1→1, 256

→3, 256 6 Convolution2D 15, 15, 256 3

→3, 256 6 卷积 2D 15, 15, 256 3

Convolution2D 15, 15, 1024 1→1, 1024

卷积 2D 15, 15, 1024 1→1, 1024

conv5 block

conv5 块

Convolution2D 8, 8, 512 1→1, 512

卷积 2D 8, 8, 512 1→1, 512

→3, 512 3Convolution2D 8, 8, 512 3

→3, 512 3convolution2d 8, 8, 512 3

Convolution2D 8, 8, 2048 1→1, 2048

卷积 2D 8, 8, 2048 1→1, 2048

pooling AveragePooling2D 1, 1, 2048 flatten Flatten 2048 dense Dense 256 relu dropout Dropout 256

池平均池 2D 1, 1, 2048 展平 2048 密集密集 256 relu 压差 256

dense Dense 1 sigmoid

致密致密 1 乙状结肠

Table 1: The structure of the modified ResNet-50.The "repetition" column indicates the number of times the block appears in the network, and the default value is 1.

表 1:改进的 ResNet-50 的结构。“重复”列指示该块在网络中出现的次数，默认值为 1。

4.2 Preparation of Input Data

4.2 输入数据的准备

Since CNNs need images as the input, the MC events after digitization need to be converted to images.We converted each event to an image of 60→60 pixels with the PNG format.For each readout signal by the vertically/horizontally arranged strips, its coordinate of (x, z)/(y, z) was mapped to the image coordinates (X, Y), and corresponding energy was encoded in the red/green color channel.In this way the two projections were merged into one picture.The center of the image was chosen to be the energy-weighted center of the hits to ensure most of the energy of the event could be encoded in the image.Each pixel in an image represents an area of 3 → 3 mmin the xz and yz planes of the corresponding event, so the total area is 180 → 180 mm. An example of such a mapping is shown in Fig. 3.

由于有线电视新闻网需要图像作为输入，数字化后的监控事件需要转换成图像。我们将每个事件转换成 PNG 格式的 60→60 像素图像。对于垂直/水平排列的条带的每个读出信号，其坐标(X, z)/(y, z)被映射到图像坐标(X, Y)，并且相应的能量被编码在红色/绿色通道中。这样，这两个投影就合并成了一幅画。图像的中心被选择为命中的能量加权中心，以确保事件的大部分能量可以被编码在图像中。图像中的每个像素代表在相应事件的 xz 和 yz 平面上的 3→3 MMI 的区域，因此总面积为 180 → 180 mm。这种映射的例子示于图 3 中。

We generated 5.6 → 10images from simulated NLDBD signal events and 5.6 → 10images from the high energy gamma background events.Within these images, 80% (training set) are used for the

我们从模拟的 NLDBD 信号事件中生成了 5.6 幅→10 图像，从高能伽马背景事件中生成了 5.6 幅→10 图像。在这些图像中，80%(训练集)用于

A comparison of models we have used can be found in Appendix B.

我们使用的模型的比较可以在附录 b 中找到

5

5

(a)

(a)

(d)

(d)

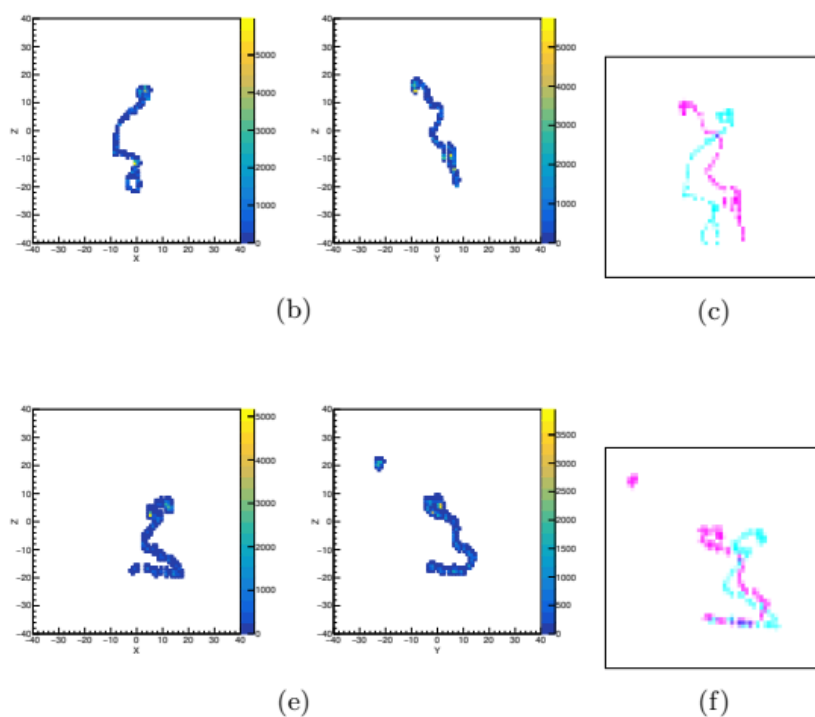


Figure 3: Examples of mapping from recorded events to images. Top: Xe NLDBD event; Bottom: Gamma background event from Bi. (a) and (d): The raw Monte Carlo 3D hits map. (b) and (e): The xz and yz projection of the event after reconstruction. (c) and (f): The resulting images for training. For better visualization, color inversion and enhancement were applied to the final images. The cyan color stands for the red channel, and the magenta color for the green channel.

图 3: 从记录的事件到图像的映射示例。顶部: Xe NLDBD 事件; 底部: 铋的伽马背景事件。(一)和(四): 原始蒙特卡洛 3D 点击率图。(b)和(e): 重建后事件的 xz 和 yz 投影。(三)和(六): 培训产生的图像。为了更好的可视化, 颜色反转和增强被应用于最终图像。青色代表红色通道, 洋红色代表绿色通道。

training of the CNN, 10% (validation set) are used for the validation, and remain 10% (testing set) are used for the checking of the power of discrimination.

有线电视新闻网的培训中, 10%(验证集)用于验证, 其余 10%(测试集)用于检查辨别能力。

4.3 Results of Event Discrimination

4.3 事件辨别的结果

The modified ResNet-50 was trained with the training set on a workstation with two NVidia GeForce 1080 GPUs for 30 epochs. To prevent overfitting and use the input data more efficiently, real-time data augmentation, such as the random operations of rotation, shifting and shearing, have been applied to the training images. The network parameters were updated in each epoch. The value of "accuracy", defined as the ratio between the number of correctly recognized events over the total number of events with the threshold of 0.5, is a measurement of the agreement of model prediction in comparison with the data. We plot the training and validation accuracies in Fig. 4. The network became overfitting apparently after the 20th epoch due to the validation accuracy became smaller than the training accuracy, though the difference is small. The training accuracy and validation accuracy are nearly identical from the 16th to 20th epoch, and the relative differences are smaller than 0.1%. To avoid the bias introduced by the arbitrary selection of models, we used all the trained models from the 16th to 20th epochs in following study.

改装后的 ResNet-50 在一个工作站上用两套 NVidia GeForce 1080 通用处理器进行了 30 个时代的训练。为了防止过度拟合和更有效地使用输入数据，对训练图像应用了实时数据增强，例如旋转、移位和剪切的随机操作。网络参数在每个时期都被更新。“准确度”值定义为正确识别的事件数量与阈值为 0.5 的事件总数之间的比率，是模型预测与数据一致性的度量。我们在图 4 中绘制了训练和验证的准确性。由于验证精度变得小于训练精度，网络在 20 世纪后明显过度拟合，尽管 difference 很小。从 16 世纪到 20 世纪，训练精度和验证精度几乎相同，相对 differences 小于 0.1%。为了避免模型的任意选择所带来的偏差，我们在后续研究中使用了 16 至 20 世纪所有经过训练的模型。

The trained models were used to classify the images in the testing set. For each input image, the output value (θ) is a number between 0 and 1, representing how it looks like a background (0) and a signal (1). The distributions of (θ) for NLDBD signal and backgrounds from model-16 (trained model in the 16th epoch) are shown in Fig. 5.

训练好的模型用于对测试集中的图像进行分类。对于每个输入图像，输出值(θ)是一个介于 0 和 1 之间的数字，表示它看起来像背景(0)和信号(1)。图 5 示出了 NLDBD 信号的(θ)分布和来自模型-16(第 16 世纪的训练模型)的背景。

A cutting threshold can be applied on the distribution to obtain the signal and background efficiency. The efficiency curves for signal and background events of model-16 at different cut values are given in Fig. 6. The selection of the threshold can be optimized by the definition of figure of merit (FOM). The commonly defined FOM is proportional to the ratio between the final number of signal events s and the square root of final number of background events b , or

可以在分布上应用切割阈值来获得信号和背景效率。图 6 给出了模型 16 在不同切割值下的信号和背景事件的效率曲线。阈值的选择可以通过品质因数的定义来优化(FOM)。通常定义的 FOM 与信号事件的最终数量 s 和背景事件的最终数量 b 的平方根之间的比率成比例，或者

$$FOM / \sqrt{s b} = s / \sqrt{b} \propto \epsilon_{s,cnn} / \sqrt{\epsilon_{b,cnn}}$$

$$\text{联邦公开市场/标准普尔} = \epsilon_{s,cnn} / \sqrt{\epsilon_{b,cnn}}$$

(1)

(1)

where $\epsilon_{s,cnn}$ and $\epsilon_{b,cnn}$ are the efficiencies for signal and background of CNN at a given cut (t_c), respectively, and s_d and b_d are the number of detected signal events and backgrounds before the CNN discrimination.

其中， $\epsilon_{s,cnn}$ 和 $\epsilon_{b,cnn}$ 分别是在给定切割(t_c)时 cnn 信号和背景的效率， s_d 和 b_d 是在 cnn 辨别之前检测到的信号事件和背景的数量。

An epoch is a complete pass through a given dataset.

纪元是对给定数据集的完整传递。

6

6

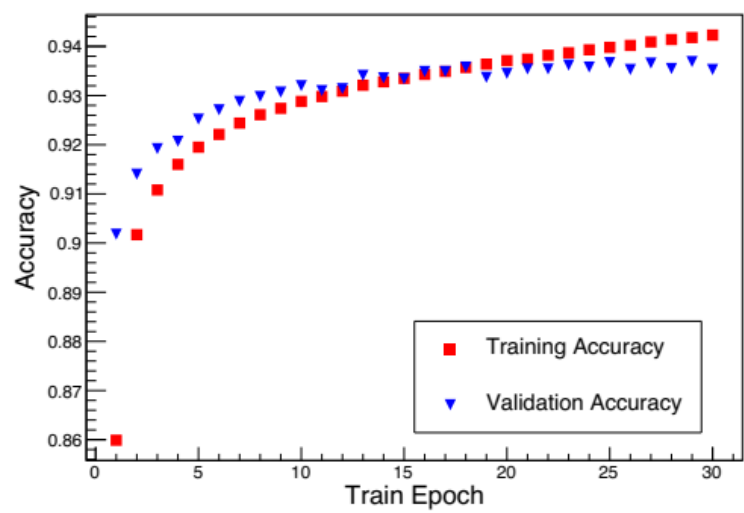


Figure 4: The evolution of the training/validation accuracy with epochs.

图 4:不同时期培训/验证准确性的演变。

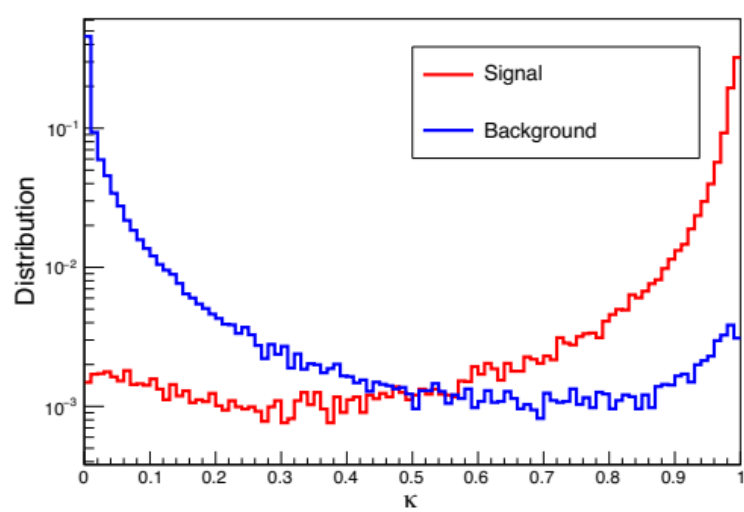


Figure 5: The distributions of θ for NLDBD signals (red) and high energy gamma backgrounds (blue) from model-16 in testing dataset. The rising of θ for backgrounds is resulted from the signal-like back-ground events.

图 5:测试数据集中来自模型 16 的 NLDBD 信号(红色)和高能伽马背景(蓝色)的 θ 分布。背景 θ 的崛起是由类似信号的背景事件造成的。

The optimized θ_c can be found by maximizing the efficiencies ratio of $\epsilon_{s,cnn}/\epsilon_{b,cnn}$. The efficiencies as functions of θ_c from model-16 is plotted in Fig. 6. The background rejection efficiency versus signal efficiency is shown in Fig. 7. The corresponding signal and background efficiencies at optimized θ_c in each model are given in Table.2.

优化的 θ_c 可以通过最大化 $\epsilon_{s,cnn}/\epsilon_{b,cnn}$ 的选优率来找到图 6 中绘出了模型-16 中 θ_c 函数的精度。背景抑制效率与信号效率的关系如图 7 所示。表中给出了每个模型在优化 θ_c 时相应的信号和背景效率。2.

We obtained different signal efficiency and background rejection efficiency with the trained network in different epochs. The final background index has been suppressed by a factor larger than 100 in all the models. The relative error of the efficiency ratio $\epsilon_{s,cnn}/\epsilon_{b,cnn}$ is only 0.09%, indicating the stability of the discrimination and should be treated as the systematic error from model selection. The reconstructed energy spectra of signal and background events before and after the optimal cut θ_c from model-16 are plotted in Fig. 8. The shape of correctly identified signal events is similar to that before the classification.

我们在不同时代通过训练有素的网络获得了不同信号效率和背景抑制效率。在所有模型中，最终背景指数都被抑制了一个大于 100 的因子。 $\epsilon_{s,cnn}/\epsilon_{b,cnn}$ 识别率的相对误差仅为 0.09%，表明识别的稳定性，应视为模型选择的系统误差。在图 8 中绘出了从模型-16 最佳切割 θ_c 之前和之后的信号和背景事件的重构能谱。正确识别的信号事件的形状与分类前相似。

Examples of falsely identified events are given in Fig. 9. The two expected Bragg peaks are not evident in the miss identified signal events. But in the falsely identified background, one could easily recognize relative large energy depositions at the two ends of the tracks.

图 9 给出了错误识别事件的例子。两个预期的布拉格峰值在未识别的信号事件中不明显。但是在错误识别的背景下，人们可以很容易地识别出轨道两端相对较大的能量沉积。

We also generated a small dataset by simulating the high energy gamma resulting from the U and Th contamination in the steel bolts. Nearly identical background rejection power is achieved by applying the trained network to the dataset. That demonstrates that the initial position of background gamma has no visible effect on the discrimination power of CNN.

我们还通过模拟钢螺栓中铀和钍污染产生的高能伽马射线生成了一个小数据集。通过将训练好的网络应用于数据集，可以获得几乎相同的背景抑制能力。这表明背景 γ 的初始位置在 CNN 的分辨力上没有可见的 effect。

According to the PandaX-III CDR, the expected background suppression factor by the traditional topological method is 35. The comparison between it and the CNN method is given in Table.4. The CNN method improves the efficiency ratio greatly, thus the detection sensitivity will be improved

根据 PanDax-iiiCDR，传统拓扑方法的预期背景抑制因子为 35。它与有线电视新闻网方法的比较见表。4.有线电视新闻网方法大大提高了效率，从而提高了检测灵敏度

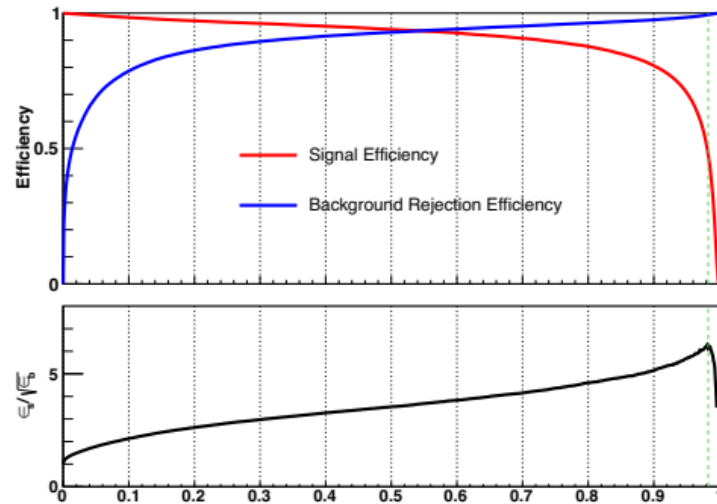


Figure 6: Top: The signal efficiency $\epsilon_{s,\text{cnn}}$ (red) and the background rejection efficiency $1 - \epsilon_{b,\text{cnn}}$ (blue) as a function of t_c from model-16. Bottom: The efficiency ratio $\epsilon_{s,\text{cnn}} / p \epsilon_{b,\text{cnn}}$ as a function of t_c from model-16. The optimized t_c is plotted as a green dashed line.

图 6: 上图: 信号效率 $\epsilon_{s,\text{cnn}}$ (红色) 和背景抑制效率 $1 - \epsilon_{b,\text{cnn}}$ (蓝色) 是模型 16 中 t_c 的函数。底部: 模型 16 中作为 t_c 函数的 $\epsilon_{s,\text{cnn}} / p \epsilon_{b,\text{cnn}}$ 系数。优化的 t_c 被绘制成绿色虚线。

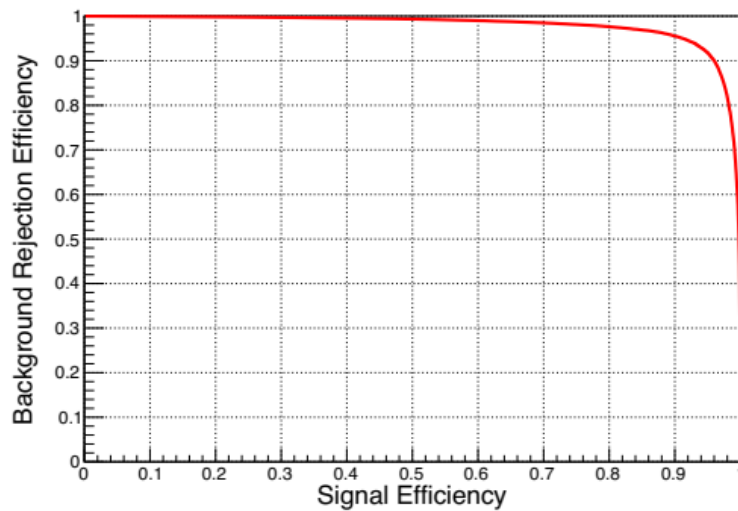


Figure 7: The background rejection efficiency $1 - \epsilon_{b,\text{cnn}}$ versus the signal efficiency $\epsilon_{s,\text{cnn}}$ from model-16.

图 7: 背景拒绝效率 $1 - \epsilon_{b,\text{cnn}}$ 与模型 16 的信号效率 $\epsilon_{s,\text{cnn}}$ 。

8

8

epoch optimized t_c $\epsilon_{s,\text{cnn}}$ $\epsilon_{b,\text{cnn}}$ $\epsilon_{s,\text{cnn}} / p \epsilon_{b,\text{cnn}}$ final BI

新纪元优化的 t_c $\epsilon_{s,\text{cnn}}$ $\epsilon_{b,\text{cnn}}$ $\epsilon_{s,\text{cnn}} / p \epsilon_{b,\text{cnn}}$ 最终 BI

16 0.983 0.475 0.9943 6.264 1.775 → 10
 16 0.983 0.475 0.9943 6.264 1.775→10
 17 0.976 0.569 0.9916 6.196 2.605 → 10
 17 0.976 0.569 0.9916 6.196 2.605→10
 18 0.981 0.487 0.9936 6.098 1.968 → 10
 18 0.981 0.487 0.9936 6.098 1.968→10
 19 0.966 0.540 0.9923 6.165 2.369 → 10
 19 0.966 0.540 0.9923 6.165 2.369→10
 20 0.976 0.520 0.9928 6.145 2.215 → 10
 20 0.976 0.520 0.9928 6.145 2.215→10
 average 6.174 0.055
 平均 6.174±0.055

Table 2: The optimized θ_c , corresponding signal efficiency $\epsilon_{s,cnn}$, background rejection efficiency $1/\epsilon_{b,cnn}$, the ratio of $\epsilon_{s,cnn}/p\epsilon_{b,cnn}$ and final BI (count kg keV year).The BI before the CNN

表 2:优化的 θ_c ，相应的信号效率 $\epsilon_{s,cnn}$ ，背景抑制效率 $1/\epsilon_{b,cnn}$ ， $\epsilon_{s,cnn}/p\epsilon_{b,cnn}$ 和最终 BI 的比率 (计数 kg keV 年)。有线电视新闻网前的商业智能

discrimination is 3.088 → 10count kg keV year[5].

歧视是 3.088→10 公斤凯文·[5]。

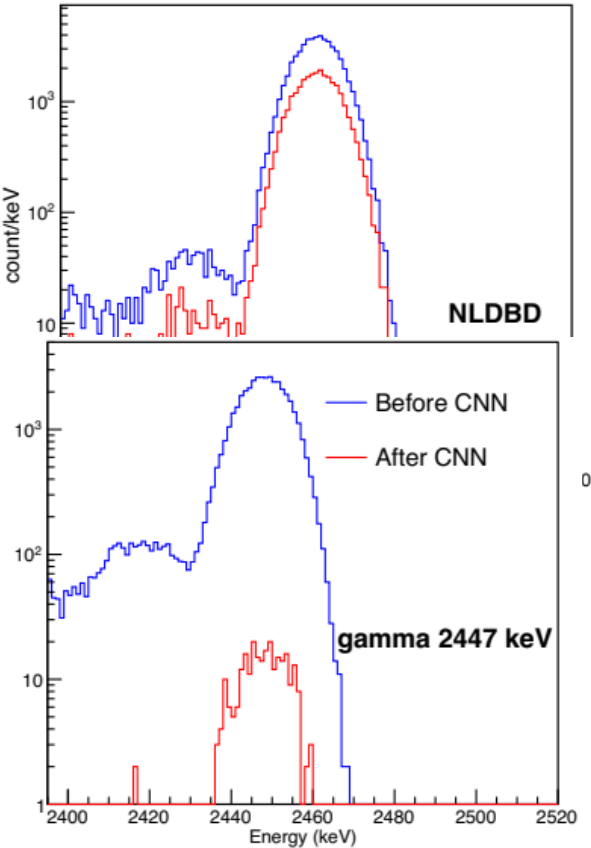


Figure 8: The reconstructed energy spectra of signal and backgrounds before and after the optimal cut (θ_c) from model-16. left: NLDBD signal events; right: background events from Bi. The spectra are not normalized.

图 8:从模型-16 最佳切割 θ_c 前后信号和背景的重构能谱。左:NLDBD 信号事件；右:毕的背景事件。光谱没有标准化。

accordingly. The large number of parameters in the CNN method helps to describe the features of physical events better in comparison with the traditional methods.

因此。与传统方法相比，有线电视新闻网方法中的大量参数有助于更好地描述物理事件的特征。

5 Summary

5 摘要

We studied the method for the discrimination of signal and background with CNN in the PandaX-III experiment based on Monte Carlo simulation. By training a modified ResNet-50 model with digitized MC data which contains only the xz and yz snapshot information, we successfully achieved a relatively high efficiency ratio of $\epsilon_{s,cnn}/\epsilon_{b,cnn}$, which improves the corresponding ratio from PandaX-III CDR with topological method by about 62%. Further studies are required to incorporate with the detector readout response, such as the signal formation for a better description of the experimental data.

在基于蒙特卡罗模拟的 panDax-iii 实验中，研究了有线电视新闻网对信号和背景的识别方法。通过使用仅包含 xz 和 yz 快照信息的数字化 MC 数据训练一个改进的 ResNet-50 模型，我们成功地获得了相对较高的 $\epsilon_{s,cnn}/\epsilon_{b,cnn}$ 准确率，用拓扑方法将 PandaX-III CDR 的对应率提高了约 62%。为了更好地描述实验数据，需要进一步研究探测器读出响应，如信号形成。

PandaX-III baseline CNN (model-16) CNN (model-18) CNN (average) ϵ_s 0.645 0.475 0.487 1 ϵ_b 0.9714 0.9943 0.9936 ϵ_s/ϵ_b 3.816 6.264 6.098 6.174 improvement - 64.2% 59.8% 61.8%

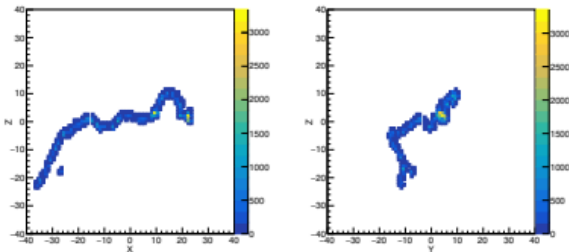
PandaX-III 基线 CNN(型号-16) CNN(型号-18) CNN(平均值) ϵ_s 0.645 0.475 0.487 1 ϵ_b 0.9714 0.9943 0.9936 ϵ_s/ϵ_b 3.816 6.264 6.098 6.174 改善- 64.2% 59.8% 61.8%

Table 3: Comparison between the results from PandaX-III baseline requirement and the CNN method.

表 3:潘达克斯-iii 基线要求和美国有线电视新闻网方法的结果比较。

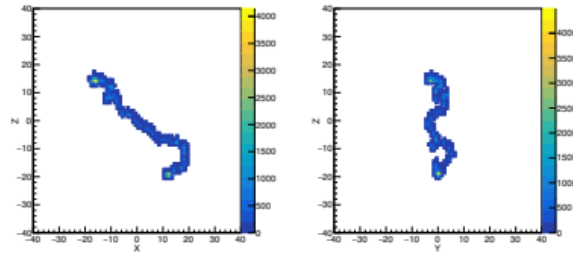
9

9



(a)

(a)



(b)

(b)

Figure 9: Falsely identified events by CNN in epoch 16.(a) The xz and yz projection of a NLDBD signal event, which is identified as a background event.(b): The xz and yz projection of a background event, which is identified as a signal event.

图 9:美国有线电视新闻网在 16 世纪错误识别的事件。被确定为背景事件的 NLDBD 信号事件的 xz 和 yz 投影。背景事件的 xz 和 yz 投影, 被识别为信号事件。

Acknowledgments

感谢

This works is supported by the grant from the Ministry of Science and Technology of China (No. 2016YFA0400302) and the grants from National Natural Sciences Foundation of China (No. 11505122 and No. 11775142).We thank the support from the Key Laboratory for Particle Physics, Astro-physics and Cosmology, Ministry of Education.This work is supported in part by the Chinese Academy of Sciences Center for Excellence in Particle Physics (CCEPP).

本作品得到中国科技部(2016YFA0400302)和国家自然科学基金(11505122 和 11775142)的资助。我们感谢教育部粒子物理、天体物理和宇宙学重点实验室的支持。这项工作得到了中国科学院粒子物理卓越中心的部分支持。

References

参考

[1] F. T. Avignone, III, S. R. Elliott, and J. Engel, Rev. Mod.Phys. 80, 481-516 (2008).

[1]阿维尼翁, 三, 艾略特和恩格尔, 修订版。Phys. 80, 481-516 (2008)。

[2] A. Gando et al. (The KamLAND-Zen collaboration), Phys. Rev. Lett.117, 082503 (2016).

[2]甘多等人(卡姆兰-禅宗合作), 列特物理牧师。117, 082503 (2016)。

[3] J. B. Albert et al. (The EXO-200 collaboration), Nature 510, 229-234 (2014).

- [3]艾伯特等人(EXO-200 合作), 自然 510, 229-234 (2014)。
- [4] V. Alvarez et al. (The NEXT collaboration), JINST 7, T06001 (2012).
- [4]诉阿尔瓦雷斯等人(下一次合作), JINST 7, T06001 (2012)。
- [5] X. Chen et al. (The PandaX-III collaboration), Sci.China Phys. Mech.Astron.60, 061011 (2017).
- [5]陈十等(潘大世合作), 科学。中国物理机械公司。阿斯顿。 60, 061011 (2017)。
- [6] S. Cebrian, T. Dafni, H. Gomez, D. C. Herrera, F. J. Iguaz, I. G. Irastorza, G. Luzon, L. Segui, and A. Tomas, J. Phys. G 40, 125203 (2013).
- [6] S. Cebrian, T. Dafni, H. Gomez, D. C. Herrera, F. J. Iguaz, I. G. Irastorza, G. Luzon, L. Segui 和 A. Tomas, J. Phys. G 40, 125203 (2013)。
- [7] P. Ferrario et al. (The NEXT collaboration), JHEP 01, 104 (2016).
- [7]费拉里奥等人(下一次合作), JHEP 01, 104 (2016)。
- [8] P. Baldi, K. Bauer, C. Eng, P. Sadowski, and D. Whiteson, Phys. Rev. D 93, 094034 (2016).
- [8]巴尔迪、鲍尔、英格、萨多夫斯基和怀特森, 《物理》第 93 版, 094034 (2016)。
- [9] J. Barnard, E. N. Dawe, M. J. Dolan, and N. Rajcic, Phys. Rev. D 95, 014018 (2017).
- [9]巴纳德、道、多兰和拉杰契奇, 《物理》第 95 版, 第 014018 页(2017 年)。
- [10] A. Aurisano, A. Radovic, D. Rocco, A. Himmel, M. D. Messier, E. Niner, G. Pawloski, F. Psihas, A. Sousa, and P. Vahle, JINST 11, P09001 (2016).
- [10]奥里萨诺、拉多维奇、罗科、希梅尔、梅西埃、尼尼微、帕洛斯基、普西阿斯、索萨和瓦勒, JINST 11, P09001 (2016)。
- [11] P. T. Komiske, E. M. Metodiev, and M. D. Schwartz, JHEP 01, 110 (2017).
- [11]科米斯克、梅托迪耶夫和施瓦茨, JHEP 01, 110 (2017)。
- [12] C. F. Madrazo, I. H. Cacha, L. L. Iglesias, and J. M. de Lucas, arXiv:1708.07034 (2017).
- [12]马德拉索、卡查、伊格莱西亚斯和卢卡斯, arXiv:1708.07034 (2017)。
- [13] R. Haake, in 2017 European Physical Society Conference on High Energy Physics (EPS-HEP 2017) Venice, Italy, July 5-12 (2017), volume EPS-HEP2017, (2017).
- [13]哈克(R. Haake), 2017 年欧洲物理学会高能物理会议(EPS-HEP2017), 意大利威尼斯, 7 月 5-12 日(2017), 卷 EPS-HEP 2017, (2017)。
- [14] H. Luo, M. Luo, K. Wang, T. Xu, and G. Zhu, arXiv:1712.03634 (2017)
- [14]罗汉忠, 罗明忠, 王克旺, 徐天成, 朱建国, arXiv:1712.03634 (2017)

- [15] J. Renner et al. (The NEXT collaboration), JINST 12, T01004 (2017).
- [15] J. Renner 等人(下一次合作), JINST 12, T01004 (2017)。
- [16] X. Cao et al. (The PandaX-I collaboration), Sci.China Phys. Mech.Astron.57, 1476-1494 (2014).
- [16]曹某等人(潘大一合作), 科学。中国物理机械公司。阿斯顿。57, 1476-1494 (2014)。
- [17] A. Tan et al. (The PandaX-II collaboration), Phys. Rev. D 93, 122009 (2016).
- [17]阿坦等人(《潘达克斯-第二次合作》), 物理杂志第 93 期, 122009 年(2016 年)。
- [18] I. G. Irastorza et al. JCAP 1601, 033 (2016).
- [18]伊拉斯托扎等人, JCAP 1601, 033 (2016 年)。
- [19] S. Agostinelli et al. Nucl.Instrum.Meth.A 506, 250-303 (2003).
- [19]阿戈斯蒂内利等人努克。仪器。冰毒。A 506, 250-303 (2003 年)。
- [20] J. Allison et al. (The GEANT4 collaboration), IEEE Trans.Nucl.Sci.53, 270 (2006).
- [20]艾利森等人(GEANT4 合作), IEEE Trans .努克尔。Sci。53, 270 (2006)。
- [21] O. A. Ponkratenko, V. I. Tretyak, and Y. G. Zdesenko, Phys. Atom.Nucl.63, 1282-1287 (2000).
- [21]奥·阿·庞克拉滕科, 《物理原子》。努克尔。63, 1282-1287 (2000)。
- [22] E. Aprile and T. Doke, Rev. Mod.Phys. 82, 2053-2097 (2010).
- [22]阿普里尔和多克, 修订版。Phys. 82, 2053-2097 (2010)。
- [23] <http://magboltz.web.cern.ch/magboltz/>,
- [23]<http://magboltz.web.cern.ch/magboltz/>,

10

10

x1

x1

x2

x2

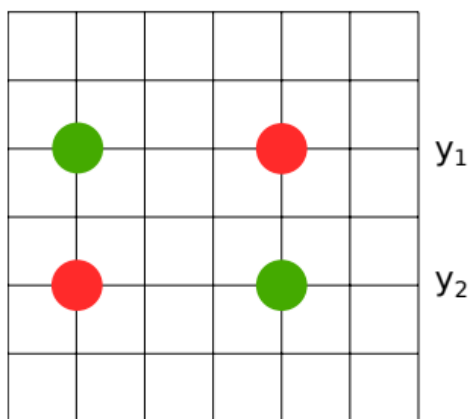


Figure 10: An example of the ambiguity in the position reconstruction with strip readout. The true positions of hits are (x_1, y_1) and (x_2, y_2) (green dots). Because all the x_1, x_2, y_1, y_2 strips have been fired, additional fake hits of (x_1, y_2) and (x_2, y_1) may be reconstructed (red dots).

图 10: 带读出的位置重建中模糊性的一个例子。点击的真实位置是 (x_1, y_1) 和 (x_2, y_2) (绿点)。因为所有 x_1, x_2, y_1, y_2 条都被发射, 所以 (x_1, y_2) 和 (x_2, y_1) 的附加假命中可以被重建 (红点)。

[24] <https://garfieldpp.web.cern.ch/garfieldpp/>,

[24] <https://garfieldpp.web.cern.ch/garfieldpp/>,

[25] A. Krizhevsky, I. Sutskever, and G. E. Hinton, in Advances in Neural Information Processing Systems 25, edited by F. Pereira, C. J. C. Burges, L. Bottou, and K. Q. Weinberger (Curran Associates, Inc. (2012)), pp. 1097-1105 (2012).

[25] 克里热夫斯基、苏斯基弗和辛顿, 《神经信息处理系统的进展》25, 由佩雷拉、伯格、博图和温伯格编辑(柯伦联合公司(2012))。第 1097-1105 页(2012 年)。

[26] M. D. Zeiler and R. Fergus, CoRR, abs/1311.2901 (2013).

[26] 泽勒博士和弗格斯博士, CoRR, abs/1311.2901 (2013)。

[27] K. Simonyan and A. Zisserman, CoRR, abs/1409.1556 (2014).

[27] 西蒙扬和塞塞曼, CoRR, abs/1409.1556 (2014)。

[28] K. He and J. Sun, CoRR, abs/1412.1710 (2014).

[28] 贺金海和孙俊杰, CoRR, abs/1412.1710 (2014)。

[29] K. He, X. Zhang, S. Ren, and J. Sun, CoRR, abs/1512.03385 (2015).

[29] 何可欣、张晓明、任善宁和孙建国, CoRR, abs/1512.03385 (2015)。

[30] F. Chollet et al. Keras, <https://github.com/keras-team/keras> (2015).

[30] 乔莱特等人, <https://github.com/keras-team/keras> 克拉斯(2015 年)。

A The ambiguity of position reconstruction with strip

带条位置重建的模糊性

readout

读出

The MicroMegas modules used by PandaX-III are read out with strips. Simultaneously hits on different strips can be used to reconstruct the positions of the signal. But ambiguity appears when more than 2 strips are fired at the same time, and an example is visualized in Fig. 10.

潘达克斯-iii 使用的微型模块用条读出。同时，不同条上的点击可以用于重建信号的位置。但是当两个以上的条被同时发射时，模糊出现，并且在图 10 中可视化了一个例子。

B Comparison between three CNN models

三种有线电视新闻网模式的比较

We have tested several different CNN structures for the discrimination of signal and background with a smaller training data set. A comparison between the model complexity, best training accuracy and the signal efficiency at a fixed background rejection efficiency for the testing data is given in Table 4. The ResNet-50 is finally chosen due to its highest signal efficiency.

我们用较小的训练数据集测试了几个不同 CNN 结构的信号和背景辨别能力。表 4 给出了模型复杂性、最佳训练精度和测试数据在固定背景抑制效率下的信号效率之间的比较。ResNet-50 因其最高的信号效率而最终被选中。

Model number of trainable parameters accuracy \Rightarrow s

可训练参数的型号精度 \Rightarrow s

3-Layer Convolutional Model 720, 993 82% 35.7%

三层卷积模型 720, 993 82% 35.7%

VGG-16[27] 15, 894, 849 92.8% 73.9%

VGG 16[27]15, 894, 849 92.8% 73.9%

ResNet-50 24, 059, 393 94.0% 79.0%

ResNet-50 24, 059, 393 94.0% 79.0%

Table 4: Simple comparison between different CNN models with a smaller training dataset. The signal efficiency \Rightarrow s is calculated at a fixed background rejection efficiency of 98.0%.

表 4: 不同 CNN 模型与较小训练数据集之间的简单比较。信号 \Rightarrow s 效率是在 98.0% 的固定背景抑制效率下计算的。

